Coarse graining, compressibility and thermal fluctuation scaling in Dissipative Particle Dynamics employed with pre-determined input parameters

N. Mai-Duy[a,*], N. Phan-Thien[b], T.Y.N. Nguyen[a] and T. Tran-Cong[a]
[a]School of Mechanical and Electrical Engineering,
University of Southern Queensland, Toowoomba, QLD 4350, Australia
[b] Department of Mechanical Engineering, Faculty of Engineering,
National University of Singapore, 9 Engineering Drive 1, 117575, Singapore.

Submitted to *Physics of Fluids*, April 2020; Revised, May 2020

ABSTRACT: In this study a Dissipative Particle Dynamics (DPD) method is employed with its input parameters directly determined from the fluid properties, such as the fluid mass density, water compressibility and viscosity. The investigation of thermal fluctuation scaling requires constant fluid properties, and this proposed DPD version meets this requirement. Its numerical verifications in simple or complex fluids under viscometric or non-viscometric flows indicate that (i) the level of thermal fluctuations in the DPD model for both types of fluids is consistently reduced with increasing in coarse-graining level; and (ii) viscometric or non-viscometric flows of a model fluid at different coarse-graining levels have a similar behaviour. Furthermore, to reduce the compressibility effect of the DPD fluid in simulating incompressible flows, a new simple treatment is presented and shown to be very effective.

Keywords: Dissipative particle dynamics (DPD), complex fluids, physical input parameters, coarse-graining, scaling, compressibility

*Corresponding author E-mail: nam.mai-duy@usq.edu.au, Telephone +61-7-46312748, Fax +61-7-46312529

1 INTRODUCTION

Dissipative Particle Dynamics (DPD) method is a simulation technique designed for modelling complex fluids, primarily in the mesoscale domains [1-4]. In this scheme, the system is thermally equilibrated through a thermostat formed by the dissipative and random forces. DPD conserves momentum locally and therefore preserves hydrodynamics. The method has been used to simulate various fluid systems, for example, particulate suspensions [5,6,7], microfluidic systems [8], red blood cells [9], thixotropic materials [10], polymer solutions [11], nanoporous shales [12], to name a few. In DPD, the solvent phase is simply modelled by a set of particles (called DPD particles) under their Newton second law motions, while the suspended phases (*e.g.,* solid particles, droplets, bubbles and polymer chains) can all be constructed from the DPD particles through appropriate constraints. With its simplicity, there are several issues in the DPD method related to (i) a fixed equation of state; (ii) no formal way of deriving DPD from an atomistic system for simple fluids (unbonded atoms); (iii) non-isothermal equations needs to be handled carefully; (iv) scaling of thermal fluctuations may be inconsistent; and (v) specification of fluid properties is not physically clear [13,14,15,16]. There have been many attempts made to improve the standard DPD formulation. For example, the many-body DPD was introduced by Pagonabarraga and Frenkel [17] to produce an arbitrary equation of state. To deal with non-isothermal problems, the energy conserving DPD was developed by Bonet Avalos and Mackie [18] and Español [19] independently. Mai-Duy *et al.* [20,21] made use of analytic expressions from the kinetic theory due to [4] (see also [22]) to derive good estimates for the fluid viscosity, compressibility, its time-scale ratio and its dynamic response – these fluid properties can now be specified as input parameters to the DPD fluid. Note that the viscosity and mass density here are defined in terms of DPD units which are the mass of a single DPD particle ($\overline{m}$), force cut-off radius ($\overline{r}_c$) and thermal energy ($\overline{k_B T}$).

As a particle-based method, DPD may suffer from the effect of compressibility. The compressibility of a DPD fluid was investigated in several works. For example, in [23], it was

observed that, due to the compressibility effect, the DPD prediction of the drag force acting on a sphere is no longer accurate when the Reynolds number is greater than 100. In [24], the coherent structures of the transition to turbulence in compressible shear flows with DPD was investigated, where the speed of sound in a DPD fluid is obtained by measuring the speed of propagation of a density pulse. In [25], two test models were proposed, where both the density and the divergence of the velocity field are considered. It was reported that the condition of constant density and divergence-free of velocity can be approximately achieved at large values of the repulsion parameter. In [26], reducing the particles' mass was shown to be an effective way to induce an incompressible slow viscous flow in a DPD fluid and simultaneously enhance its dynamic response.

DPD is a coarse-graining technique for the simulation of fluids at the mesoscale, where hydrodynamics and thermos fluctuations have a role. There was concern that the process of coarse-graining in DPD has its upper limit that would prevent the method from widespread use. By taking into account the dependence of the parameters in the model on the level of coarse-graining, the DPD and the many-body DPD were shown to be truly mesocopic methods in [27] and [28], respectively. With the scaling schemes presented in [27,28], the DPD methods can be applied to any desired length scale, where different physical systems can share some physical properties such as compressibility (but not viscosity, to be discussed later).

It should be pointed out that the DPD can be employed in its generalised hydrodynamic regime, where the transport coefficients are dependent on the wavelengths and frequencies of thermal fluctuations and through which finite-size effects can be taken into account [29,30,31].

In this work, we will examine numerically the "physical input" version of DPD, and focus on its coarse graining and scaling, and its compressibility. In the study of thermal fluctuation scaling, the fluid properties (e.g., mass density, compressibility and viscosity) should remain invariant with respect to the coarse-graining level. We will show that this requirement can be met by scaling the original DPD inputs in a way that can make the pre-determined input

values unchanged. It is observed that the thermal fluctuations reduce in magnitude with higher coarse-graining levels, and the flows of a model fluid at different coarse-graining levels are demonstrated to have a similar behaviour. In this work, the compressibility of the model fluid is matched to that of water. To reduce unwanted compressibility effects, a simple way based on the time-scale ratio is proposed and shown to be very effective.

The remainder of the paper is organised as follows. A brief review of DPDs with classical and explicit input parameters is given in Section 2. The coarse graining process is shown to achieve a consistent thermal fluctuation scaling in Section 3, and its flow behaviour and some means of reducing unwanted compressibility effects of the DPD fluid are presented and discussed in Sections 4 and 5, respectively. Section 6 gives some concluding remarks.

2 DPD

2.1 Classical DPD

In DPD, the fluid is modelled by a system of particles undergoing their Newton 2nd law motions [1,2]:

$$m\ddot{\mathbf{r}}_i = m_i\dot{\mathbf{v}}_i = \sum_{j=1,j\neq i}^{N} (\mathbf{F}_{ij,C} + \mathbf{F}_{ij,D} + \mathbf{F}_{ij,R}) + \mathbf{F}_{i,e}, \tag{1}$$

where m, $\mathbf{r}_i$ and $\mathbf{v}_i$ represent the mass, position vector and velocity vector of a particle i, $i = 1, \ldots, N$, respectively, N is the total number of particles, the superposed dot denotes a time derivative, $\mathbf{F}_{i,e}$ is an external force on particle i, and the first three forces on the right side represent the conservative (subscript C), the dissipative (subscript D) and the random

forces (subscript R):

$$\mathbf{F}_{ij,C} = a_{ij} w_C \mathbf{e}_{ij}, \tag{2}$$

$$\mathbf{F}_{ij,D} = -\gamma w_D \left(\mathbf{e}_{ij} \cdot \mathbf{v}_{ij}\right) \mathbf{e}_{ij}, \tag{3}$$

$$\mathbf{F}_{ij,R} = \sigma w_R \theta_{ij} \mathbf{e}_{ij}, \quad w_R = \sqrt{w_D}, \quad \sigma = \sqrt{2\gamma k_B T}. \tag{4}$$

Here, a_{ij} (a scalar), γ and σ are constants reflecting the strengths of these forces, w_C, w_D and w_R configuration-dependent weighting functions, $\mathbf{e}_{ij} = \mathbf{r}_{ij}/r_{ij}$ a unit vector from particle j to particle i ($\mathbf{r}_{ij} = \mathbf{r}_i - \mathbf{r}_j$, $r_{ij} = |\mathbf{r}_{ij}|$), $\mathbf{v}_{ij} = \mathbf{v}_i - \mathbf{v}_j$ a relative velocity vector, θ_{ij} a Gaussian white noise, T the (absolute) temperature, and k_B the Boltzmann constant ($k_B T$ the thermal energy). All these interaction forces are pairwise, centre-to-centre, and zero outside a cutoff radius r_c. An example of the external force is gravity (body force), which is often used to simulate the effect of a pressure gradient. It is noted that the random force is introduced in such a way to guarantee the satisfaction of the fluctuation-dissipation theorem [2]. In practice, the equations of motion (1) are solved in reduced units; one can take, for example, $m = 1$, $r_c = 1$ and $k_B T = 1$.

There are three time scales in the stochastic differential equation (1) [22]:

- a fluctuation time scale τ_R of the random force, which is arbitrarily small,
- an inertia time scale $\tau_I = O\left(m\gamma^{-1}\right)$,
- and a relaxation time scale $\tau = O\left(\gamma H^{-1}\right)$, where H is the stiffness of the system, $H = O(|\partial_r F_C|) = O\left(a_{ij} r_c^{-1}\right)$.

The flow domain is divided into a set of fixed small bins to collect results from numerically solving the DPD equations of motion (1). Data collected in each bin include the velocities, forces and the number of entries of the DPD particles. The averaging process is then carried out to produce the flow properties (*e.g.,* number density, fluid density and linear momentum).

The stress tensor is computed using the Irving-Kirkwood formula and the pressure can be found from the trace of the stress tensor [4].

In the classical DPD method, a standard choice of the weighting functions is $w_C = (1-r/r_c)$ and $w_D = (1-r/r_c)^2$, and the input parameters include a_{ij}, σ, k_BT, m, n (particle density) and r_c. Note that γ is not an independent input parameter ($\gamma = \sigma^2/(2k_BT)$). In general, any modification of the input DPD parameters can result in a change of the fluid properties (*e.g.,* viscosity). In particular, by changing n while keeping all the other variables unchanged, the resultant DPD system represents a different fluid, which makes the characteristic study of DPD (*e.g.,* scaling of thermal fluctuations) difficult.

2.2 DPD with explicit input parameters

In the proposed DPD here, the fluid viscosity, compressibility, dynamics response and time-scale ratio can be specified in advance, as discussed in [20,21]. For the sake of completeness, basic formulas of the physical input version of DPD [20,21] are reproduced below.

The weighting function for conservative forces is chosen as $w_C = (1-r/r_c)^{\bar{s}}$. The two free parameters, a_{ij} and $\bar{s}$ in function w_C, are designed to satisfy given values of the time-scale ratio α [21] and dimensionless compressibility κ^{-1} [32,33,27], according to

$$\alpha = \frac{\tau}{\tau_I} = \frac{\gamma^2 r_c}{m a_{ij}}, \tag{5}$$

$$\kappa^{-1} = \frac{1}{k_B T n \kappa_T} = \frac{1}{k_B T}\frac{\partial p}{\partial n}. \tag{6}$$

In (5), τ and τ_I are defined in the previous section. The time-scale ratio α can be utilised to keep the dissipative and conservative forces balanced; its values can be acquired from some numerical experiments in simple flows [21]. In (6), n is the number density, κ_T the isothermal compressibility, p the pressure and $\kappa^{-1} = 15.98$ for water. Note that $n = n_{phys}/\nu$, where n_{phys} is the molecular number density and ν the number of molecules per DPD particle

(coarse-graining level). The system, (5) and (6), can be solved analytically for the two variables a_{ij} and $\bar{s}$, given α and κ^{-1},

$$a_{ij} = \frac{1}{\alpha}\frac{\gamma^2 r_c}{m}, \tag{7}$$

$$\bar{s} = \frac{\sqrt{5+4\sqrt{C+1}}-5}{2}, \quad C = \frac{8\pi a_{ij} n r_c^4}{(\kappa^{-1}-1)k_B T}. \tag{8}$$

It is noted that $\partial p/\partial n$ in (6) is explicitly expressed in terms of the cut-off radius, resulting in C as a function of r_c.

The weighting function for dissipative forces is chosen as $w_D = (1-r/r_c)^{1/2}$ [34]. Here, we are interested in the case of high damping limit, where collisions are mainly due to the dissipative and random forces. This limit is thought to be relevant to the general DPD case. From the kinetic theory, there are two contributions to the viscosity, kinetic part and dissipative part. When the dissipative contribution is dominant, the input/specified viscosity, namely η, of the DPD system can be imposed by enforcing the following constraint

$$\overline{\eta}_D = \frac{\gamma n^2 [R^2 w_D]_R}{30} = \eta, \tag{9}$$

in which $\overline{\eta}_D$ is the dissipative viscosity predicted by the kinetic theory and $[R^2 w_D]_R \equiv \int d\mathbf{R} R^2 w_D(R) = 1024\pi r_c^5/3465$. This equation can be solved for the variable γ:

$$\gamma = \frac{51975\eta}{512\pi n^2 r_c^5}. \tag{10}$$

If the Schmidt number/speed of sound is taken as an additional input to the DPD equation (1), the weighting function for dissipative forces is employed in the form of $(1-r/r_c)^s$. One can then use the two parameters s and γ to match the viscosity and dynamic response

$$\overline{\eta}_D = \eta, \tag{11}$$

$$\frac{\overline{\eta}}{\rho D} = S_c, \quad D = \frac{2\overline{\eta}_K}{\rho}, \quad \overline{\eta} \simeq \overline{\eta}_D, \quad \rho = mn, \tag{12}$$

where S_c is the Schmidt number, and $\overline{\eta}_K$ and $\overline{\eta} = \overline{\eta}_K + \overline{\eta}_D$ are the kinetic viscosity and the viscosity predicted by the kinetic theory. In this case, the parameters s and γ take the form

$$s = \frac{-9 + \sqrt{1 + 4C}}{2}, \quad C = \frac{6 S_c m k_B T n^2 r_c^2}{5\eta^2}, \tag{13}$$

$$\gamma = \frac{5\eta(s+1)(s+2)(s+3)(s+4)(s+5)}{16\pi n^2 r_c^5}. \tag{14}$$

It is noted that contributions from the conservative forces to the viscosity are neglected here. However, as shown in [20], when the repulsion parameter is chosen from the condition of water-like compressibility, and high values of the input viscosity (values correspond to $s < 2$, s: the exponent in the dissipative weighting function) are employed, the differences between the measured viscosities, where the conservative forces are included and the viscosities predicted by the kinetic theory are shown to be less than about 4%. In the present work, relatively high values of the imposed viscosity are chosen and all simulations are conducted with the inclusion of conservative forces.

3 COARSE GRAINING AND SCALING

In the DPD, one typically employs the mass of a single DPD particle, force cut-off radius and thermal energy as basic units. The time, mass, length and viscosity of the system are thus not defined explicitly but in terms of these DPD units. We use the superposed bar to denote a dimensional quantity and define the unit of mass, length and energy as $\overline{m}$, $\overline{r}_c$ and $\overline{\varepsilon} = \overline{k_B T}$, respectively.

In Füchslin *et al.* [27], a physical system represented by $\overline{N}_{phys}$ molecular particles is to be scaled (coarse-grained) at different levels ν so that one deals with a smaller number of particles

$$\overline{N} = \frac{\overline{N}_{phys}}{\nu}, \tag{15}$$

in which $\nu = \overline{N}_{phys}/\overline{N}$ is referred to as a coarse-graining level. Two different coarse-graining levels are considered, ν and ν' (modelled by $\left\{\overline{N}, \overline{k_BT}, \overline{n}, \overline{m}, \overline{r}_c, \overline{a}, \overline{\gamma}\right\}$ and $\left\{\overline{N}', \overline{k_BT}', \overline{n}', \overline{m}', \overline{r}_c', \overline{a}', \overline{\gamma}'\right\}$, respectively). Their relations in three dimensions are established as ($\phi = \nu'/\nu$ is the scaling)

$$\begin{aligned} &\overline{N}' = \phi^{-1}\overline{N}, \quad \overline{k_BT}' = \phi\overline{k_BT}, \quad \overline{n}' = \phi^{-1}\overline{n}, \\ &\overline{m}' = \phi\overline{m}, \qquad \overline{r}_c' = \phi^{1/3}\overline{r}_c, \qquad \overline{\tau}' = \phi^{1/3}\overline{\tau}, \\ &\overline{a}' = \phi^{2/3}\overline{a}, \qquad \overline{\gamma}' = \phi^{2/3}\overline{\gamma}, \qquad \overline{\sigma}' = \phi^{5/6}\overline{\sigma}, \end{aligned} \tag{16}$$

where $\overline{\tau}$ and $\overline{\tau}'$ are time scales. With these scalings, it can be shown that DPD is a scale-free (truly mesoscopic) method.

One may rewrite equation (1) without external forces in the following dimensional differential form

$$\Delta\overline{\mathbf{r}}_i = \overline{\mathbf{v}}_i\Delta\overline{t}, \tag{17}$$

$$\begin{aligned} \overline{m}\Delta\overline{\mathbf{v}}_i = &\sum_j \overline{a}_{ij} w_C\left(\overline{r}_{ij}\right)\mathbf{e}_{ij}\Delta\overline{t} - \sum_j \overline{\gamma} w_D\left(\overline{r}_{ij}\right)\left(\mathbf{e}_{ij}\cdot\overline{\mathbf{v}}_{ij}\right)\mathbf{e}_{ij}\Delta\overline{t} \\ &+ \sum_j \overline{\sigma} w_R\left(\overline{r}_{ij}\right)\theta_{ij}\mathbf{e}_{ij}\sqrt{\Delta\overline{t}}. \end{aligned} \tag{18}$$

Let's scale length by $\overline{r}_c$, mass by $\overline{m}$, and time by $\overline{\tau}$ (which later chosen as $(\overline{r}_c\sqrt{\overline{m}/\overline{k_BT}})$ and define dimensionless variables:

$$\widehat{m} = \frac{\overline{m}}{\overline{m}} = 1, \quad \widehat{\mathbf{r}} = \frac{\overline{\mathbf{r}}}{\overline{r}_c}, \quad \widehat{t} = \frac{\overline{t}}{\overline{\tau}}, \quad \frac{d}{d\overline{t}} = \frac{d}{\overline{\tau}d\widehat{t}}, \quad \widehat{\mathbf{v}} = \frac{\overline{\tau}}{\overline{r}_c}\overline{\mathbf{v}}. \tag{19}$$

Dimensional equations of motion (17) and (18) then reduce to

$$\Delta\widehat{\mathbf{r}}_i = \widehat{\mathbf{v}}_i \Delta\widehat{t}, \tag{20}$$

$$\begin{aligned}\widehat{m}\Delta\widehat{\mathbf{v}}_i = &\sum_j \frac{\overline{a}_{ij}\overline{\tau}^2}{\overline{m}\,\overline{r}_c} w_C\left(\widehat{r}_{ij}\right)\mathbf{e}_{ij}\Delta\widehat{t} - \sum_j \frac{\overline{\gamma}\,\overline{\tau}}{\overline{m}} w_D\left(\widehat{r}_{ij}\right)\left(\mathbf{e}_{ij}\cdot\widehat{\mathbf{v}}_{ij}\right)\mathbf{e}_{ij}\Delta\widehat{t} \\ &+ \sum_j \frac{\overline{\sigma}\,\overline{\tau}^{3/2}}{\overline{m}\,\overline{r}_c} w_R\left(\widehat{r}_{ij}\right)\theta_{ij}\mathbf{e}_{ij}\sqrt{\Delta\widehat{t}}.\end{aligned} \tag{21}$$

By defining new dimensionless parameters as

$$\widehat{a}_{ij} = \frac{\overline{a}_{ij}\overline{\tau}^2}{\overline{m}\,\overline{r}_c},\ \ \widehat{\gamma} = \frac{\overline{\gamma}\,\overline{\tau}}{\overline{m}},\ \ \widehat{\sigma} = \frac{\overline{\sigma}\,\overline{\tau}^{3/2}}{\overline{m}\,\overline{r}_c}, \tag{22}$$

they further reduce to

$$\Delta\widehat{\mathbf{r}}_i = \widehat{\mathbf{v}}_i \Delta\widehat{t}, \tag{23}$$

$$\begin{aligned}\widehat{m}\Delta\widehat{\mathbf{v}}_i = &\sum_j \widehat{a}_{ij} w_C\left(\widehat{r}_{ij}\right)\mathbf{e}_{ij}\Delta\widehat{t} - \sum_j \widehat{\gamma} w_D\left(\widehat{r}_{ij}\right)\left(\mathbf{e}_{ij}\cdot\widehat{\mathbf{v}}_{ij}\right)\mathbf{e}_{ij}\Delta\widehat{t} \\ &+ \sum_j \widehat{\sigma} w_R\left(\widehat{r}_{ij}\right)\theta_{ij}\mathbf{e}_{ij}\sqrt{\Delta\widehat{t}}.\end{aligned} \tag{24}$$

with the thermal equilibrium requiring

$$2\overline{k_BT}\,\overline{\gamma} = \overline{\sigma}^2.$$

Making use of the last two expressions in (22) and also $\widehat{k_BT} = \overline{k_BT}/\overline{\varepsilon} = \overline{k_BT}/\overline{k_BT} = 1$, the requirement becomes

$$2\widehat{k_BT}\,\overline{k_BT}\,\widehat{\gamma}\frac{\overline{m}}{\overline{\tau}} = \widehat{\sigma}^2\frac{\overline{m}^2\overline{r}_c^2}{\overline{\tau}^3}.$$

Thus the scaling

$$\overline{\tau} = \overline{r}_c\sqrt{\frac{\overline{m}}{\overline{k_BT}}} \tag{25}$$

will guarantee the thermal equilibrium of the DPD system (23)-(24):

$$2\widehat{k_BT}\widehat{\gamma} = \widehat{\sigma}^2. \tag{26}$$

It can be seen that every system with the same values of

$$\widehat{a}_{ij} = \frac{\overline{a}_{ij}\overline{r}_c}{\overline{k_BT}}, \;\; \widehat{\gamma} = \frac{\overline{\gamma}\,\overline{r}_c}{\left(\overline{m}\,\overline{k_BT}\right)^{1/2}}, \;\; \widehat{\sigma}^2 = \frac{\overline{\sigma}^2\overline{r}_c}{\overline{m}^{1/2}\overline{k_BT}^{3/2}} \tag{27}$$

will have the same state space. Making use of (16), the three dimensionless parameters scale as

$$\frac{\overline{a}'_{ij}\overline{r}'_c}{\overline{k_BT}'} = \phi^{2/3+1/3-1}\frac{\overline{a}_{ij}\overline{r}_c}{\overline{k_BT}} = \frac{\overline{a}_{ij}\overline{r}_c}{\overline{k_BT}}, \tag{28}$$

$$\frac{\overline{\gamma}'\overline{r}'_c}{\left(\overline{m}'\overline{k_BT}'\right)^{1/2}} = \phi^{2/3+1/3-1/2-1/2}\frac{\overline{\gamma r}_c}{\left(\overline{m}\overline{k_BT}\right)^{1/2}} = \frac{\gamma\overline{r}_c}{\left(\overline{m}\overline{k_BT}\right)^{1/2}}, \tag{29}$$

$$\frac{\overline{\sigma}'^2\overline{r}'_c}{\overline{m}'^{1/2}\overline{k_BT}'^{3/2}} = \phi^{5/3+1/3-1/2-3/2}\frac{\overline{\sigma}^2\overline{r}_c}{\overline{m}^{1/2}\overline{k_BT}^{3/2}} = \frac{\overline{\sigma}^2\overline{r}_c}{\overline{m}^{1/2}\overline{k_BT}^{3/2}}, \tag{30}$$

indicating that the two coarse-graining systems are stochastically equivalent. Using (16), let's examine the relations for the mass density, compressibility and viscosity, respectively,

$$\overline{\rho}' = \overline{m}'\overline{n}' = \phi^{1-1}\overline{m}\,\overline{n} = \overline{\rho} \text{ (invariant)} \tag{31}$$

$$\frac{\overline{a}'\overline{n}'\overline{r}'^4_c}{\overline{k_BT}'} = \phi^{2/3-1+4/3-1}\frac{\overline{a}\,\overline{n}\,\overline{r}^4_c}{\overline{k_BT}} = \frac{\overline{a}\,\overline{n}\,\overline{r}^4_c}{\overline{k_BT}} \text{ (invariant)} \tag{32}$$

$$\overline{\gamma}'\overline{n}'^2\overline{r}'^5_c = \phi^{2/3-2+5/3}\overline{\gamma}\,\overline{n}^2\overline{r}^5_c = \phi^{1/3}\overline{\gamma}\,\overline{n}^2\overline{r}^5_c \text{ (not invariant)} \tag{33}$$

With this scaling scheme, different coarse-graining levels will have the same mass density and compressibility but different viscosities.

In the present work, the DPD equations are solved in reduced units (of mass, force cut-off radius and thermal energy). Equations of motion (1) are employed here for simulation. There are two additional parameters ($\bar{s}$ in w_C and s in w_D), which make the relations for the

parameters between two coarse-graining levels generally more complicated than those in (16). When the particle number is reduced ($n' = \phi^{-1}n$, $\phi > 1$), we also take ($m' = \phi m$), increase the cut-off radius ($r_c' > r_c$), but keep not only the mass density and water compressibility but also the viscosity and Schmidt number (where appropriate) constant. Values of (a_{ij}, $\bar{s}$, γ, s) and (a_{ij}', $\bar{s}'$, γ', s') are derived from expressions (7), (8), (10), (13) and (14) for given sets of (k_BT, α, η, (S_c)) and (k_BT', $\alpha' = \alpha$, $\eta' = \eta$, ($S_c' = S_c$)), respectively. These scalings can be easily obtained numerically. Note that (i) $\bar{s}$ is a function of (κ, a_{ij}, n, r_c, k_BT), s a function of (S_c, η, m, n, r_c, k_BT), a_{ij} a function of (α, r_c, m, γ), and γ a function of (η, s, n, r_c); and (ii) If S_c is not a specified value, the parameter s is taken to be 1/2.

The thermal fluctuations in the present scaling scheme are studied for both simple and complex fluid systems. A consistent scaling of thermal fluctuations means that their magnitude becomes smaller with larger particle volumes [35].

3.1 Simple fluids

We consider some Newtonian fluid modelled by $\alpha = 1$, $\eta = 30$, $k_BT = 1$, water-like compressibility and constant mass density ($\rho = mn = 8$). Three coarse-graining levels employed with $n = \{8, 6, 4\}$, $m = \{1, 4/3, 2\}$ and $r_c = \{1, 1.1006, 1.2599\}$ are taken to represent the model fluid. The domain is chosen as $15 \times 15 \times 15$ (in DPD units). For r_c, the scaling factor used is the same as that in (16), i.e. $\phi^{1/3}$. The volume of particles can be regarded as $V_i \sim 1/n$. The results on the distribution of the velocity component of a DPD particle are shown in Figure 1. It can be seen that the thermal fluctuations are reduced with lower number densities (larger particle sizes). Note that from the kinetic theory, the Schmidt number is estimated as 290 for $n = 8$, 319 for $n = 6$ and 365 for $n = 4$.

3.2 Particulate suspensions

We consider the suspension of a single rigid particle in a Newtonian fluid. The solvent phase is modelled with $\alpha = 1$, $\eta = 30$, $\rho = mn = 8$, $k_BT = 1$ and water compressibility, and the colloidal particle is constructed using the spring model [36]. The domain is chosen as $15 \times 15 \times 15$ (in DPD units).

In the first test, we employ 3 different coarse-graining levels with $n = \{8, 6, 4\}$, $r_c = \{1, 1.1006, 1.2599\}$ and $m = \{1, 4/3, 2\}$ for the solvent and keep the volume fraction of the suspended phase constant. For the spring model, the volume fraction is also the particle fraction because the standard/basic DPD particles are used to represent both the constituent and solvent particles. Let N_C^0 be the number of basic DPD particles used to represent the colloidal phase and N_S be the number of basic particles used for the solvent phase, the volume fraction is computed as $\phi = N_C^0/(N_C^0 + N_S)$. In the present problem (one colloidal particle), by taking the number of constituent particles per colloid as the (solvent) particle number density, the volume fraction remains invariant: $\phi = 1 \times n/(1 \times n + Vn) = 1/(1+V) = 2.96 \times 10^{-4}$ (V: the box volume) for any value of n. Using the radial distribution function (RDF) to measure the exclusion of the colloidal particle at three coarse-graining levels, they all lead to similar results - the size of the exclusion zone is about 0.475 in DPD units. The results are displayed in Figure 2, showing the change of n (solvent particle's size) does not affect the level of thermal fluctuations of the colloidal particle.

In the second test, we employ $n = 8$, $r_c = 1$, $m = 1$ and $S_c = 600$ for the solvent and the colloid of three different sizes, i.e. 6, 12 and 20 DPD particles per colloid (by means of RDF, sizes of exclusion zones are measured as 0.30, 0.36 and 0.51 in DPD units, respectively). The results are displayed in Figure 3, indicating that the thermal fluctuations of the colloid are reduced with its larger size.

For the standard DPD method, the exponents of the weighting functions in the dissipative and repulsive forces are fixed. For the present DPD method, these exponents are variables

and they are functions of the viscosity, Schmidt number, fluid compressibility and time-scale ratio. For the test in Section 3.1 (simple fluids) and the first test in Section 3.2 (particulate suspensions), different coarse-graining levels are considered. When going from one coarse-graining level to the other, one has different fluids for the standard DPD and the same fluid for the present DPD. The standard DPD is thus not directly applicable to the study of thermal fluctuation scaling for these tests. For the second test, only one coarse-graining level for the solvent is considered. The exponents of the weighting functions in the dissipative and repulsive forces all stay the same when changing the size of the colloid particle. In this regard, the present DPD can be considered as the standard DPD and these two versions are expected to produce similar results. Figure 4 shows a comparison of thermal fluctuations between the standard DPD and the present DPD. The former is employed with $n = 4, r_c = 1.5, m = 1, k_B T = 1, \bar{s} = 1, s = 1/2, \sigma = 3$ and $a_{ij} = 3.5320$, which lead to, by means of kinetic theory, $\alpha = 8.5997, \eta = 16.9721$ and $S_c = 1.6452 \times 10^2$. The latter is employed with $n = 4, r_c = 1.5, m = 1, k_B T = 1, \alpha = 8.5997, \eta = 16.9721$ and $S_c = 1.6452 \times 10^2$. Similar behaviours are obtained, and when the size of the colloidal particle is increased, thermal fluctuations of the colloid are reduced (variance: 0.1643, 0.0867 and 0.0493 for the standard DPD and 0.1661, 0.0812, 0.0492 for the present DPD).

These tests demonstrate that the present DPD method has a proper scaling with respect to its thermal fluctuations.

4 FLOWS OF THE MODEL FLUID AT DIFFERENT COARSE-GRAINING LEVELS

For the viscosity approximation taken in the form of (9), its error depends on the two quantities n and r_c. Using the kinetic theory as a guide, the total viscosity $\bar{\eta}$ of the DPD

system is computed as

$$\bar{\eta} = \frac{3}{5}\frac{\rho k_B T n r_c^2}{\eta(s+4)(s+5)} + \eta, \tag{34}$$

where η is the input viscosity and ρ is the fluid density. In (34), the first term on RHS is the kinetic viscosity, which should be designed to be negligible. As a result, for a given set of η, ρ and k_BT, one needs to reduce r_c if there is an increase in n (smaller mean distance between particles). In our numerical experiments conducted in Sections 4.1 and 4.2, the product of n and r_c as well as k_BT are kept constant. For r_c, between two coarse-graining levels, the scaling factor is chosen as ϕ.

4.1 Double Poiseuille flow

This flow is simulated in two dimensions. By dividing the domain of analysis into two equal regions by the line $y = 0$ and then assigning an acceleration $\mathbf{g} = (F_e/m, 0) = (1, 0)$ to each particle in the upper region ($y > 0$) and $\mathbf{g} = (-1, 0)$ to each particle in the lower region ($y < 0$), a periodic Poiseuille flow is produced with the theoretical values of the velocity and shear stress: $u_x = \rho g_x y(L_y/2 - y)/(2\eta)$ and $\tau_{xy} = \rho g_x(L_y/2 - 2y)/2$, where $0 \leq y \leq L_y/2$ and L_y is the length of the box in the y direction. The simulation results for the double Poiseuille flows are shown in Figure 5, where three different sets of $\{n, r_c, m\}$ are employed as $\{8, 1, 1\}$, $\{6, 4/3, 4/3\}$ and $\{4, 2, 2\}$ corresponding to 3200, 2400 and 1600 particles, respectively, over the flow domain. Other input parameters are $\eta = 30$, $\alpha = 1$, $k_BT = 1$, $\Delta t = 0.001$ and 300000 time steps. The domain is chosen as 20×20 (in DPD units). It can be seen from Figure 5 that both velocities and shear stresses at the three coarse-graining levels have similar behaviours and they are in a good agreement with the theoretical values.

To test accuracy of the viscosity estimation based on the kinetic theory (i.e. equation (9)) for this problem, the following second order polynomial

$$u_x(y) = -\left(\frac{\rho g_x}{2\eta}\right) y^2 + \left(\frac{\rho g_x}{2\eta}\right) y$$

is fitted to the velocity profile with $y > 0$, which returns the two coefficients from which the viscosity is computed in an average sense. The obtained viscosity is 30.5173, 30.3265 and 30.0965 for the 3 coarse-graining levels employed. With the input viscosity $\eta = 30$, the differences between the measured viscosities and the input viscosity are thus within 2%.

4.2 Flow past a periodic square array of fixed cylinders

For this type of flow, the analysis can be carried out in two dimensions. Because of its periodicity, one can replace the infinite domain with a cell volume containing one cylinder. Assume that the motion of a fluid is driven by a pressure drop in the x direction. Consider some Newtonian fluid defined by $\eta = 100$, $\rho = nm = 4$, $nr_c = 16$, $k_BT = 1$ and $\alpha = 1$. Three coarse-graining levels using relatively small values of the number density ($n = \{10, 8, 6\}$) are employed to represent the model fluid. A cell is chosen as 10×10 (in DPD units).

A cylinder is constructed with the spring model [36]. For $n = 8$, as shown in Figure 6, the number of constituent particles used to model a cylinder are chosen as 19 and they are located at the cylinder's centre and at the distances $r_1 = 0.1(1/n_x + 1/n_y)/2 = 0.1(1/2 + 1/4)/2 = 0.0375$ ($n_x n_y = n$) and $r_2 = 2r_1$, in which $(1/n_x + 1/n_y)/2$ is regarded as the mean distance between the solvent particles, and the factor 0.1 is introduced to prevent the fluid particles from penetrating the cylinder. For other values of n, cylinders are also constructed in a similar manner, except that the constituent particles are chosen in a way that the ratio of the number of constituent particles to the total number of particles in the system (particle fraction) is kept constant, i.e. 0.0232.

Fluid-fluid and fluid-cylinder radial distribution functions (RDFs) at no-flow conditions for three values of the number density are displayed in Figure 7. If the exclusion zone is defined as an area where the value of RDF is less than 0.01, then the cylinders are of similar sizes (about 0.47) and the sizes of fluid particles can be negligible. The small (negligible) size of the fluid particle is mainly due to the use of large r_c (greater than 1) as discussed in [37].

We impose a range of the body force ($F_e = \{0.01, 0.02, \cdots, 0.10, 0.12, \cdots, 0.30\}$) on the fluid particles in the x direction to drive the fluid motion. The flows here are slow with their Reynolds numbers ($Re = \rho UL/\eta$) being less than 0.2 (L and U: the distance between the cylinders and mean velocity in the x direction), the diffusion time scale $t = \rho L^2/\eta = 4$ and the convection time scale $t = L/U \simeq 20$ (for the maximum value of U). For these slow flows ($Re < 0.2$), one can have a wide choice of the size ratio of the cylinder to the solvent particle in the simulation without causing spurious behaviour, and the diffusion time scale is important as the Peclet number, which measures the ratio of the convection and the diffusion terms, is small, i.e. $P_e = \rho LU/\eta \simeq 0.2$. Figure 8 shows the effect of the imposed body force on the cylinder's size and fluid particle's size. It can be seen that the sizes of the cylinder and fluid particles are not much affected by the change in the imposed force.

Figure 9 displays the obtained drag forces on the three coarse-graining levels. It can be seen that their behaviours are similar in trend and their values are consistently closer to each other with decreasing in the mean flow velocity. As the Reynolds number is increased (larger velocity), a higher Mach number is also resulted and the compressibility effect of the DPD fluid becomes more significant (Figure 10), which can strongly affect the prediction of the drag force. The use of lower coarse-graining levels (larger values of the number density) has higher speeds of sound (lower Mach number) according to equation (36) and thus can alleviate this problem. This is probably the reason why the coarse-graining level affects the drag forces predicted here. For this type of flow, an analytic expression of the drag force derived from the solution of the Stokes equation was reported in [38]. Here, its values are referred to as theoretical ones. The DPD results are seen to be in better agreement with the theoretical values as the Reynolds number is reduced.

5 REDUCING UNWANTED COMPRESSIBILITY EFFECTS

Like any fluid that is modeled by a set of particles, a DPD fluid is compressible. Special attention is thus needed when simulating incompressible flows. In [32,26], water compressibility was enforced in the DPD system. In [26], in addition, the particles' mass was proposed to reduce in order to increase the speed of sound. In the present context (DPD with explicit inputs), compressibility of the DPD fluid is matched to that of water. We investigate the effect of using lower mass and also propose a new means that can further reduce unwanted compressibility effects.

We measure compressibility of the DPD fluid by the density residual defined as

$$\Delta n = \sqrt{\frac{\sum_{i=1}^{N_b} (n_i - n)^2}{N_b}}, \tag{35}$$

where N_b is the number of bins, n_i the number density of the ith bin and n the reference number density.

5.1 The mass approach

Expression for the speed of sound of the DPD fluid is given by [4]

$$c_s^2 = \frac{k_B T}{m} + \frac{\pi}{15} \frac{anr_c^4}{m} \tag{36}$$

If the particle's mass is reduced, it leads to a higher speed of sound as well as a lower Reynolds number and a smaller diffusion time scale. When the Mach number ($M = U/c_s$, U is a flow characteristic velocity) is less than 0.3, the flow may be regarded as an incompressible flow. On the other hand, one has to deal with overdamped (stiff) systems, for which much smaller

time steps are required for a proper simulation. This can be alleviated by means of the stochastic exponential time differencing (SETD) scheme [26]. For a given number density, reducing m leads to fluids of different mass densities.

5.2 The time-scale ratio approach

The time-scale ratio ($\alpha = \tau/\tau_I$) relates to the conservative and dissipative forces. This dimensionless quantity can thus be used to control the quantitative relation between the two forces. It will be demonstrated that varying α can lead to a significant improvement in the distribution of the number density over the flow domain. Unlike the use of low mass, the mass density of the model fluid will not be affected by the change in α.

First, we examine the performance of the SETD scheme. Consider a Couette flow with the imposed shear rate $\dot{\gamma} = 0.2$. The two plates move with the same velocity U but in opposite direction. The mass is specified as $m = 0.01$ and some other input parameters are $\eta = 100$, $n = 10$, $k_BT = 1$, $\alpha = 10$, $r_c = 1.6$ and 100 bins per a unit area. The simulations are carried out in two dimensions on the domain 10×10 (in DPD units) with 10^6 time steps. Table 1 displays computed values of the mean thermal energy by the velocity-Verlet and SETD schemes for different times steps, which show that larger time steps and better accuracy are acquired with the latter.

The obtained results concerning the number density by the mass and time-scale approaches are displayed in Figure 11 for simple flows and in Figure 12 for complex flows. Here, Couette flow is chosen as an example for simple flows. The density residual is observed to reduce with a decreasing mass (1.3568 for $m = 1$, 1.2833 for $m = 0.1$ and 1.2687 for $m = 0.01$). Taking $U = 1$ and $L = 5$ ($\dot{\gamma} = 0.2$), the Reynolds number is 0.5 for $m = 1$, 0.05 for $m = 0.1$ and 0.005 for $m = 0.01$. For a given m, by changing the value of α, it can be seen that a significant improvement in the number density distribution is achieved without affecting the fluid mass density. Also, varying α for $m = 1$ yields better results than the case of

low mass $m = 0.01$ with standard repulsion. As expected, the optimal value of $\alpha = \tau/\tau_I$ increases as the mass is reduced (smaller inertia time). For any mass employed here, a simple selection of $\alpha = 1$ is still able to lead to reasonable results when compared to the case of standard repulsion. Turning to complex flows: flow past an array of fixed cylinders, similar remarks can be made here. The Reynolds number is approximately 0.2 for $m = 1$, 0.02 for $m = 0.1$ and 0.002 for $m = 0.01$. It appears that varying α is more effective and efficient than reducing the particles' mass.

Figure 13 shows that the variations of α for simple and complex flows have similar behaviours. It can be seen that their minimum density residuals all occur in the range $\alpha = 0.01 - 1$. A simple mechanism to find the optimal value of α can thus be suggested. For a given set of DPD input parameters, the simulation is first conducted on some simple flows (*e.g.* Couette flow) and the obtained best value of α can then be utilised in the simulation of the flow of interest.

6 CONCLUDING REMARKS

In this study, the DPD simulations are conducted with the viscosity, compressibility, dynamic response (where appropriate) and time-scale ratio being specified as input parameters, from which a consistent scaling of thermal fluctuations and similar behaviours of the flow at different coarse-graining levels have been demonstrated. The issue of compressibility is also studied. Reducing the particles' mass and/or varying the time-scale ratio can reduce unwanted compressibility effects. The advantages of the time-scale ratio approach over the low mass approach are (i) one still has the same model fluid (constant viscosity, water compressibility and mass density) without the need to change other input parameters; and (ii) a much improved result for the number density distribution can be achieved. Attractive features from the use of pre-determined input parameters are expected to allow an effective DPD scheme to simulate (nearly) incompressible multiphase flows to be developed.

DATA AVAILABILITY

The data that support the findings of this study are available within the article.

REFERENCES

1. P. J. Hoogerbrugge, and J. M. V. A. Koelman, "Simulating microscopic hydrodynamic phenomena with dissipative particle dynamics," *Europhys. Lett.* **19**, 155-160 (1992).

2. P. Español, and P. B. Warren, "Statistical mechanics of dissipative particle dynamics," *Europhys. Lett.* **30**, 191-196 (1995).

3. P. Español, "Hydrodynamics from dissipative particle dynamics," *Phys. Rev. E* **52**, 1734-1742 (1995).

4. C. Marsh, *Theoretical aspect of dissipative particle dynamics* (PhD thesis) (University of Oxford, 1998).

5. W. Pan, B. Caswell, and G. E. Karniadakis, "Rheology, microstructure and migration in Brownian colloidal suspensions," *Langmuir* **26**, 133-142 (2010).

6. A. Panchenko, D. F. Hinz, and E. Fried, "Spatial averaging of a dissipative particle dynamics model for active suspensions," *Phys. Fluids* **30**, 033301 (2018).

7. Q. Nie, Y. Zhong, and H. Fang, "Study of a nanodroplet breakup through many-body dissipative particle dynamics," *Phys. Fluids* **31**, 042007 (2019).

8. Z. Li, G.-H. Hu, Z.-L. Wang, Y.-B. Ma, and Z.-W. Zhou, "Three dimensional flow structures in a moving droplet on substrate: A dissipative particle dynamics study," *Phys. Fluids* **25**, 072103 (2013).

9. T. Ye, N. Phan-Thien, B. C. Khoo, and C. T. Lim, "Dissipative particle dynamics simulations of deformation and aggregation of healthy and diseased red blood cells in a tube flow," *Phys. Fluids* **26**, 111902 (2014).

10. K. Le-Cao, N. Phan-Thien, B. C. Khoo, and N. Mai-Duy, "A dissipative particle dynamics model for thixotropic materials exhibiting pseudo-yield stress behaviour," *J. Non-Newton. Fluid Mech.* **241**, 1-13 (2017).

11. Y. Kong, C. W. Manke, W. G. Madden, and A. G. Schlijper, "Effect of solvent quality on the conformation and relaxation of polymers via dissipative particle dynamics," *J. Chem. Phys.* **107**, 592 (1997).

12. Y. Xia, J. Goral, H. Huang, I. Miskovic, P. Meakin, and M. Deo, "Many-body dissipative particle dynamics modeling of fluid flow in fine-grained nanoporous shales," *Phys. Fluids* **29**, 056601 (2017).

13. M. B. Liu, G. R. Liu, L. W. Zhou, and J. Z. Chang, "Dissipative Particle Dynamics (DPD): An Overview and Recent Developments," *Archives of Computational Methods in Engineering* **22(4)**, 529-556 (2015).

14. P. Español, and P. B. Warren, "Perspective: Dissipative particle dynamics," *J. Chem. Phys.* **146**, 150901 (2017).

15. M. Ellero, and P. Español, "Everything you always wanted to know about SDPD* (*but were afraid to ask)," *Applied Mathematics and Mechanics* **39(1)**, 103124 (2018).

16. T. Ye, D. Pan, C. Huang, and M. Liu, "Smoothed particle hydrodynamics (SPH) for complex fluid flows: Recent developments in methodology and applications," *Phys. Fluids* **31**, 011301 (2019).

17. I. Pagonabarraga, and D. Frenkel, "Dissipative particle dynamics for interacting systems," *J. Chem. Phys.* **115**, 5015-5026 (2001).

18. J. Bonet Avalos, and A. D. Mackie, "Dissipative particle dynamics with energy conservation," *Europhys. Lett.* **40**, 141 (1997).

19. P. Español, "Dissipative particle dynamics with energy conservation," *Europhys. Lett.* **40**, 631-636 (1997).

20. N. Mai-Duy, N. Phan-Thien, and T. Tran-Cong, "An improved dissipative particle dynamics scheme," *Appl. Math. Model.* **46**, 602-617 (2017).

21. N. Mai-Duy, N. Phan-Thien, and T. Tran-Cong, "Imposition of physical parameters in dissipative particle dynamics," *Comput. Phys. Comm.* **221**, 290-298 (2017).

22. N. Phan-Thien, and N. Mai-Duy, *Understanding Viscoelasticity: An Introduction to Rheology* (3rd Ed.) (Springer International Publishing, Cham, 2017).

23. J. M. Kim and R. J. Phillips, "Dissipative particle dynamics simulation of flow around spheres and cylinders at finite Reynolds numbers," *Chem. Eng. Sci.* **59(20)**, 41554168 (2004).

24. J .W. van de Meent, A. Morozov, E. Somfai, E. Sultan and W. van Saarloos, "Coherent structures in dissipative particle dynamics simulations of the transition to turbulence in compressible shear flows," *Phys. Rev. E* **78(1)**, 015701 (2008).

25. D. Pan, N. Phan-Thien, N. Mai-Duy, B. C. Khoo, "Numerical investigations on the compressibility of a DPD fluid," *J. Comput. Phys.* **242**, 196-210 (2013).

26. N. Phan-Thien, N. Mai-Duy, D. Pan, and B. C. Khoo, "Exponential-time differencing schemes for low-mass DPD systems," *Comput. Phys. Comm.* **185**, 229-235 (2014).

27. R. M. Füchslin, H. Fellermann, A. Eriksson, and H.-J. Ziock, "Coarse graining and scaling in dissipative particle dynamics," *J. Chem. Phys.* **130**, 214102 (2009).

28. M. Arienti, W. Pan, X. Li and G. Karniadakis, "Many-body dissipative particle dynamics simulation of liquid/vapor and liquid/solid interactions," *J. Chem. Phys.* **134(20)**, 204114 (2011).

29. M. Ripoll, M. H. Ernst, and P. Español, "Large scale and mesoscopic hydrodynamics for dissipative particle dynamics," *J. Chem. Phys.* **115(15)**, 7271-7284 (2001).

30. N. Phan-Thien, N. Mai-Duy, and T. Y. N. Nguyen, "A note on dissipative particle dynamics (DPD) modelling of simple fluids," *Computers and Fluids* **176**, 97-108 (2018).

31. N. Mai-Duy, T. Y. N. Nguyen, K. Le-Cao K, and N. Phan-Thien, "Investigation of particulate suspensions in generalised hydrodynamic dissipative particle dynamics using a spring model," *Applied Mathematical Modelling* **77(1)**, 652-662 (2020).

32. R. D. Groot, and P. B. Warren, "Dissipative particle dynamics: Bridging the gap between atomistic and mesoscopic simulation," *J. Chem. Phys.* **107**, 4423 (1997).

33. R. D. Groot, and K. L. Rabone, "Mesoscopic Simulation of Cell Membrane Damage, Morphology Change and Rupture by Nonionic Surfactants," *Biophysical Journal* **81**, 725-736 (2001).

34. X. Fan, N. Phan-Thien, S. Chen, X. Wu and T. Yong Ng, "Simulating flow of DNA suspension using dissipative particle dynamics," *Phys. Fluids* **18**, 063102 (2006).

35. A. Vázquez-Quesada, M. Ellero, and P. Español, "Consistent scaling of thermal fluctuations in smoothed dissipative particle dynamics," *J. Chem. Phys.* **130**, 034901 (2009).

36. N. Phan-Thien, N. Mai-Duy, and B. C. Khoo, "A spring model for suspended particles in dissipative particle dynamics," *J. Rheol.* **58**, 839-867 (2014).

37. N. Mai-Duy, N. Phan-Thien, and B. C. Khoo, "Investigation of particles size effects in Dissipative Particle Dynamics (DPD) modelling of colloidal suspensions," *Comput. Phys. Comm.* **189**, 37-46 (2015).

38. H. Hashimoto, "On the periodic fundamental solutions of the Stokes equations and their application to viscous flow past a cubic array of spheres," *J. Fluid Mech.* **5**, 317-328 (1959).

Table 1: Couette flows, $U = 1, \eta = 100, n = 10, r_c = 1.6, k_BT = 1, \alpha = 10$, simulation box with dimensions of 10×10, 100 bins per unit area and 10^6 time steps: Comparison of the mean thermal energy of the velocity-Verlet and SETD schemes for $m = 0.01$. The former fails to converge at $\Delta t \geq 2.5 \times 10^{-4}$.

	Velocity-Verlet		SETD	
Δt	$\overline{k_BT}$	Error(%)	$\overline{k_BT}$	Error(%)
5.0×10^{-4}	-	-	0.4928	50.7
2.5×10^{-4}	-	-	0.7717	22.8
1.0×10^{-4}	0.8917	10.82	0.9525	4.74
7.5×10^{-5}	0.9164	8.36	0.9723	2.76
5.0×10^{-5}	0.9422	5.78	0.9871	1.28
2.5×10^{-5}	0.9696	3.03	0.9959	0.41
1.0×10^{-5}	0.9872	1.28	0.9984	0.15

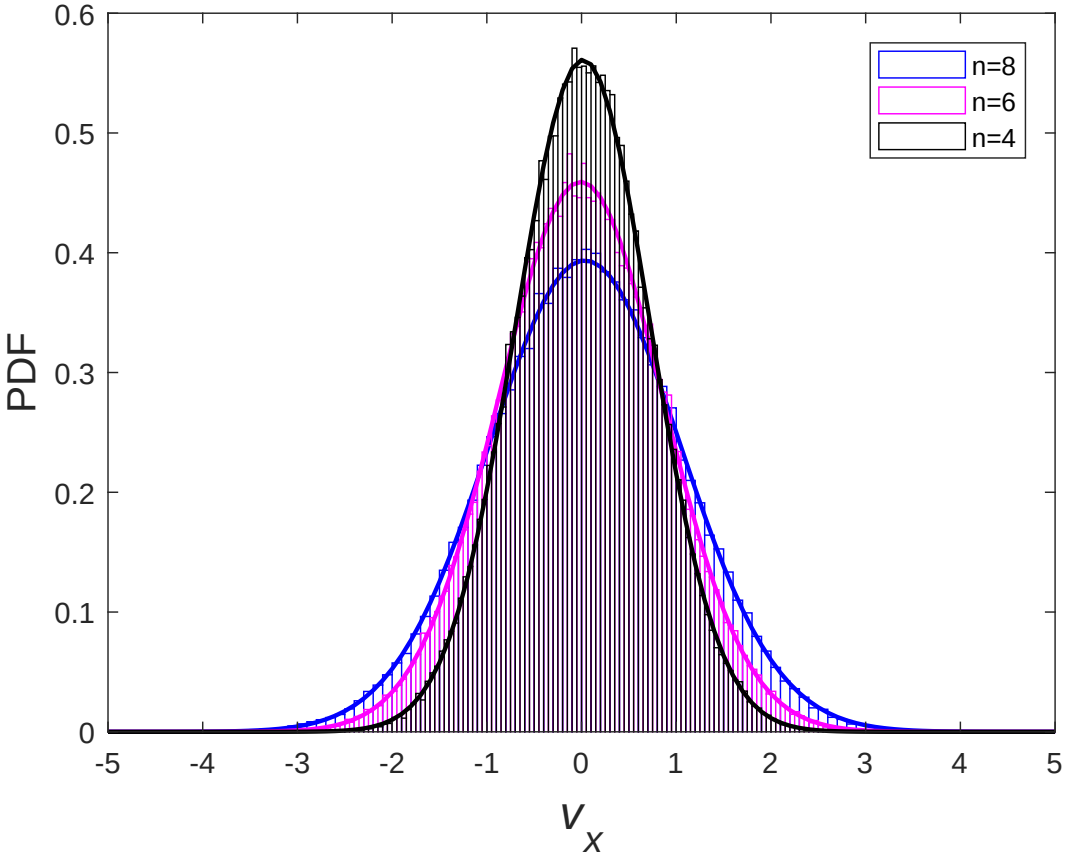

Figure 1: Simple fluid with water-like compressibility, $\alpha = 1$, $\eta = 30$ and $\rho = mn = 8$; simulation box with dimensions of $15 \times 15 \times 15$; $s = 0.5$; $k_BT = 1$; and $\Delta t = 0.001$: Probability density function (PDF) of v_x of a DPD particle at 3 different coarse-graining levels ($n = \{8, 6, 4\}$; $r_c = \{1, 1.1006, 1.2599\}$; $m = \{1, 4/3, 2\}$). Thermal fluctuations are reduced (variance: 1.0272, 0.7546, 0.5054) with larger particle size.

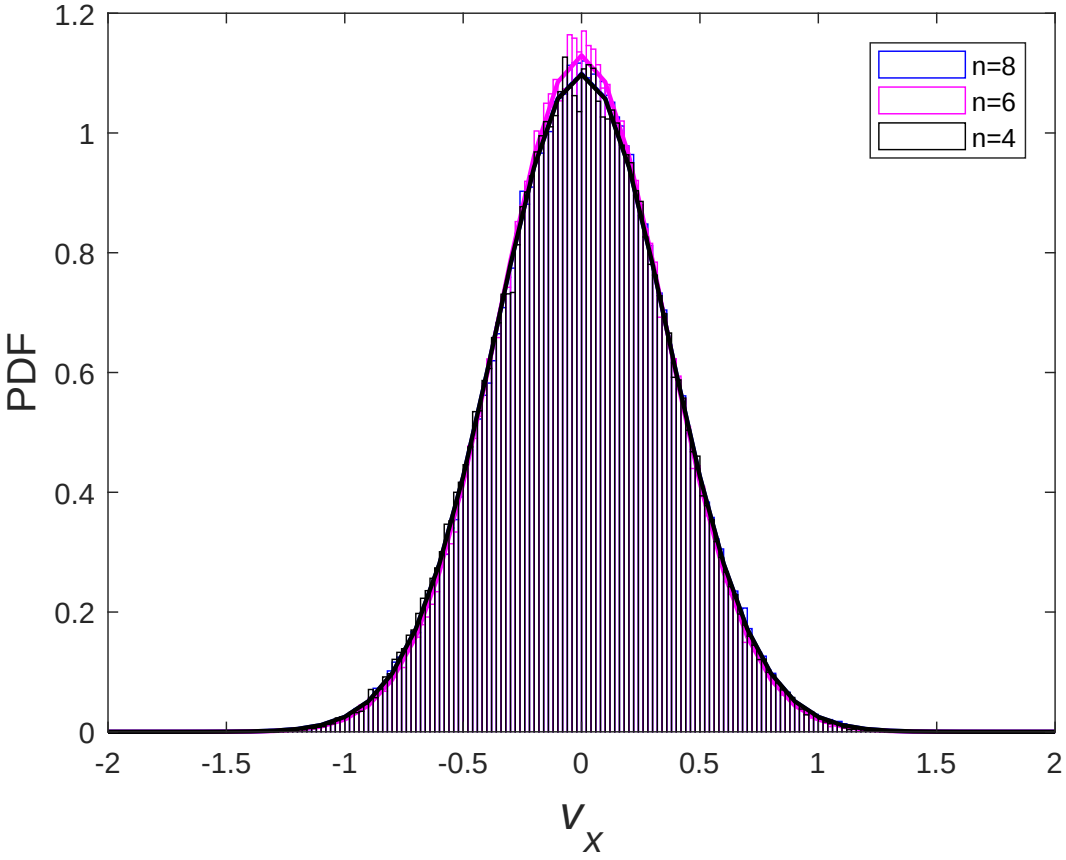

Figure 2: Suspension with water-like compressibility, $\alpha = 1$, $\eta = 30$ and $\rho = 8$ for the solvent phase; constant volume fraction for the suspended phase; simulation box with dimensions of $15 \times 15 \times 15$; $k_B T = 1$; and $\Delta t = 0.001$: Probability density function (PDF) of v_x of a single colloidal particle in the solvent employed at 3 different coarse-graining levels ($n = \{8, 6, 4\}$; $r_c = \{1, 1.1006, 1.2599\}$; $m = \{1, 4/3, 2\}$). Its computed variances are similar (0.1318, 0.1247, 0.1321).

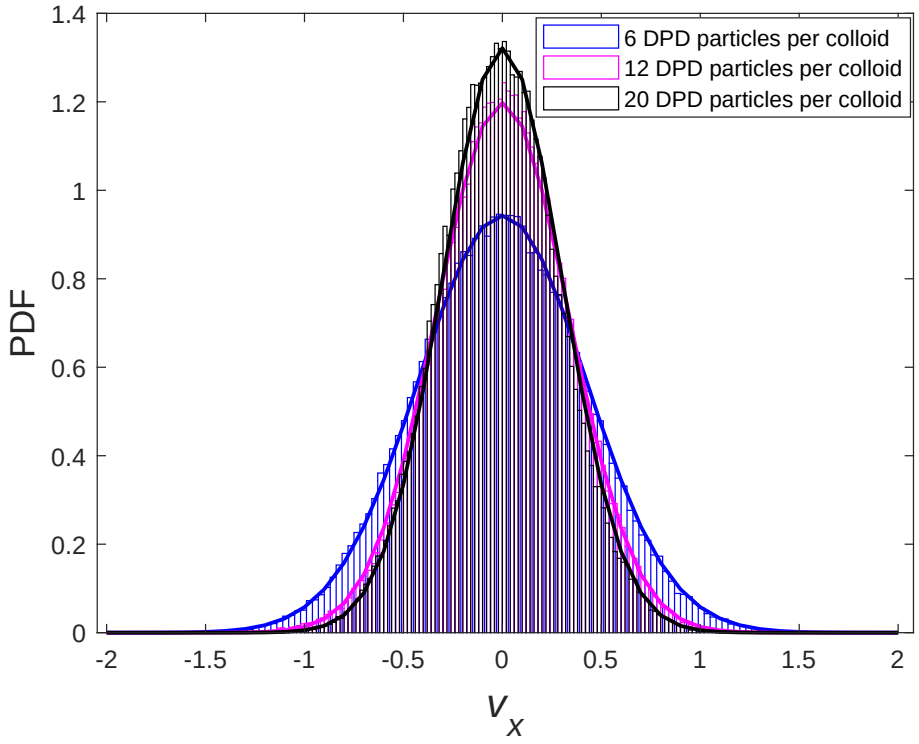

Figure 3: Suspension with the solvent phase: water-like compressibility, $\alpha = 1$, $\eta = 30$, $\rho = mn = 8$ and $S_c = 600$; simulation box with dimensions of $15 \times 15 \times 15$; $k_B T = 1$; and $\Delta t = 0.001$: Probability density function (PDF) of v_x of a single colloidal particle employed with 3 different sizes at the same solvent coarse graining level ($n = 8$, $r_c = 1$, $m = 1$). Thermal fluctuations of the colloid are reduced (variance: 0.1790, 0.1109, 0.0912) with its larger size.

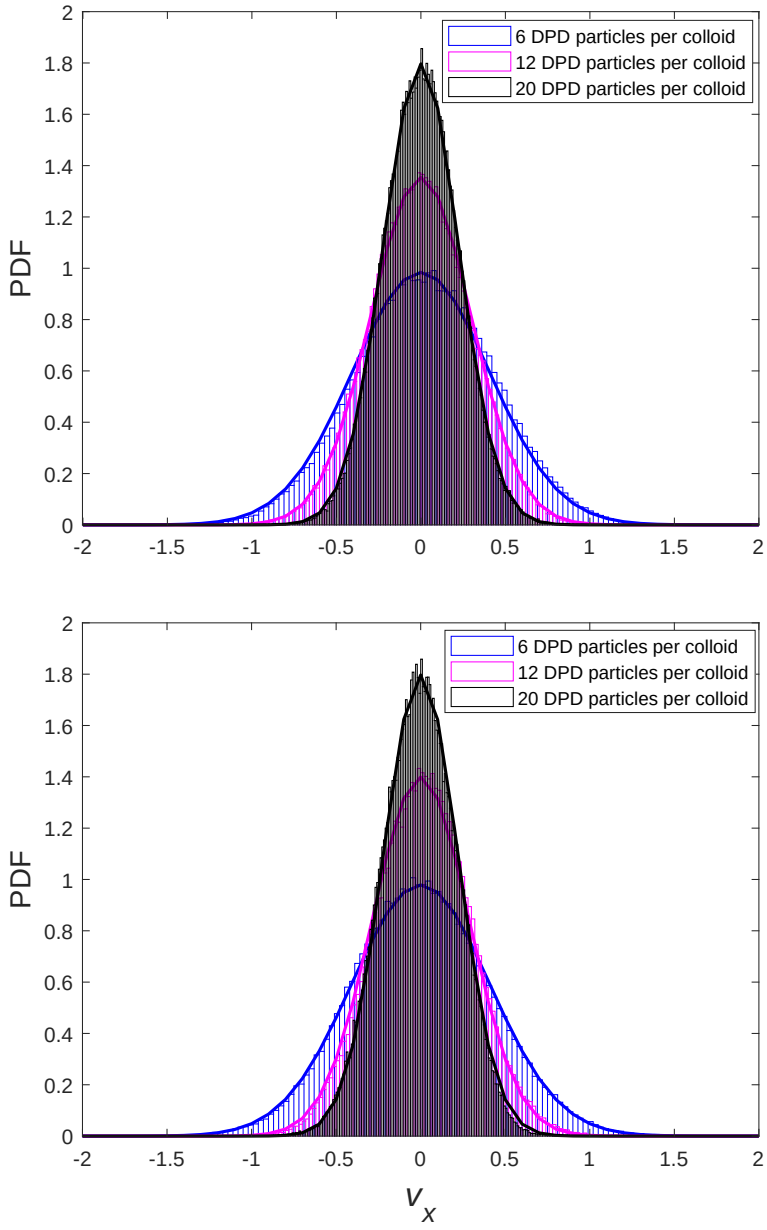

Figure 4: Probability density function (PDF) of v_x of a single colloidal particle employed with 3 different sizes at the same solvent coarse graining level by the standard (top) and present (bottom) DPDs. It can be seen that the two methods produce similar behaviours. When the size of the colloidal particle is increased, thermal fluctuations of the colloid are reduced (variance: 0.1643, 0.0867 and 0.0493 for the standard DPD and 0.1661, 0.0812, 0.0492 for the present DPD).

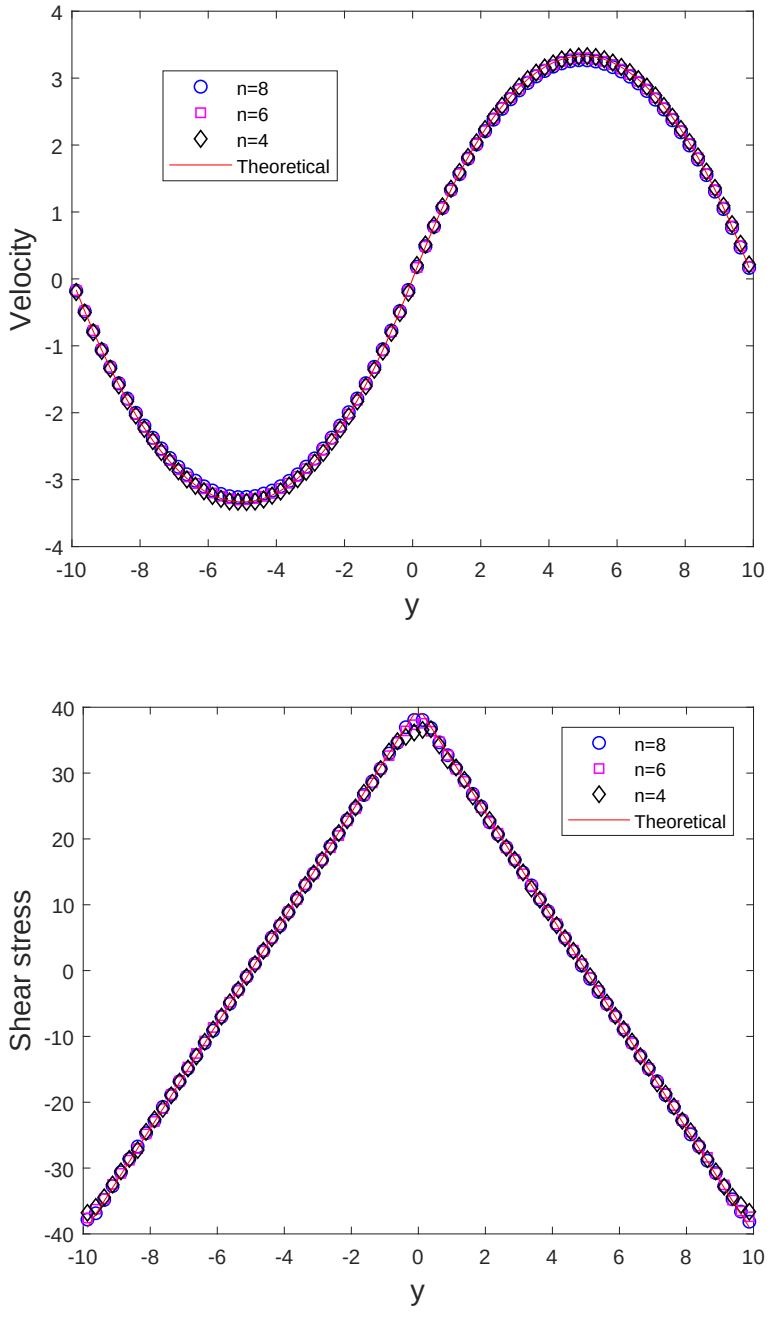

Figure 5: Poiseuille flow: Some typical results by the present DPD at $n = \{8, 6, 4\}$. Theoretical values for velocity and shear stress are also included.

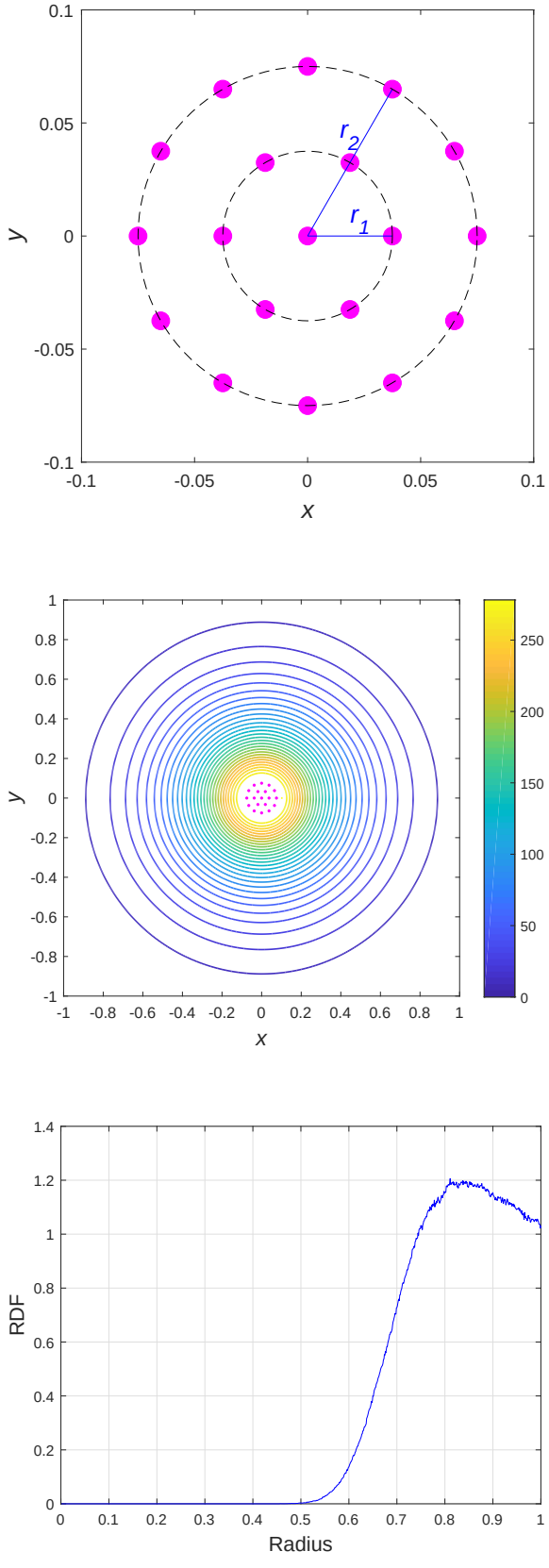

Figure 6: Modelling of the fixed cylinder with the surrounding fluid defined by $\{\eta = 100,\ n = 8,\ r_c = 2,\ m = 0.5,\ k_BT = 1,\ \alpha = 1\}$: Reference sites of constituent particles of the cylinder (top), its repulsion force field in the radial direction (middle) and fluid-cylinder radial distribution function at no-flow conditions (bottom). Note that, for both constituent and fluid particles, $F_{ij,C} = 23.96(1 - r/r_c)^{6.67}$.

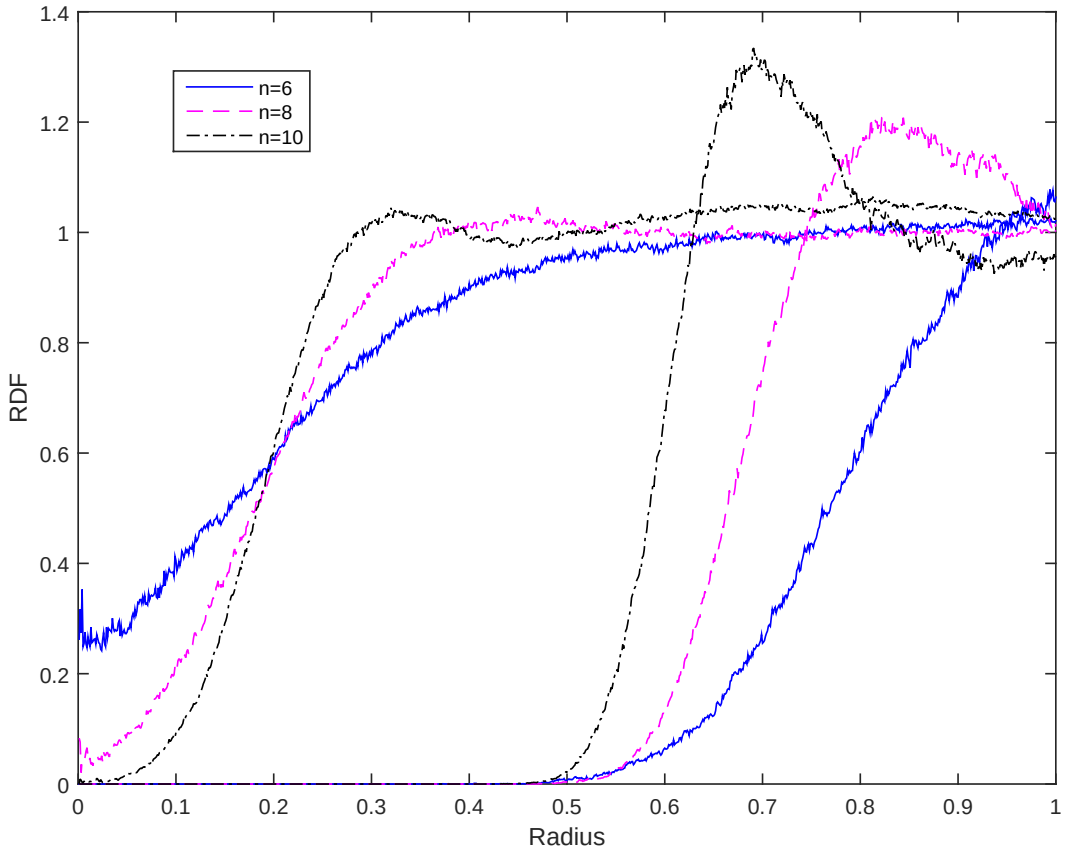

Figure 7: Flows past a periodic array of fixed cylinders: Fluid-fluid (left) and fluid-cylinder (right) radial distribution functions for different number densities at no-flow conditions: By defining the exclusion zone as an area where the RDF values are less than 0.01, the cylinders for different resolutions are of similar sizes (about 0.47), and the fluid particle sizes can be negligible. The obtained variations of fluid-cylinder RDFs imply that (i) cylinders modelled by the spring model are soft cylinders; and (ii) using lower levels of coarse graining can improve the hardness of the cylinder.

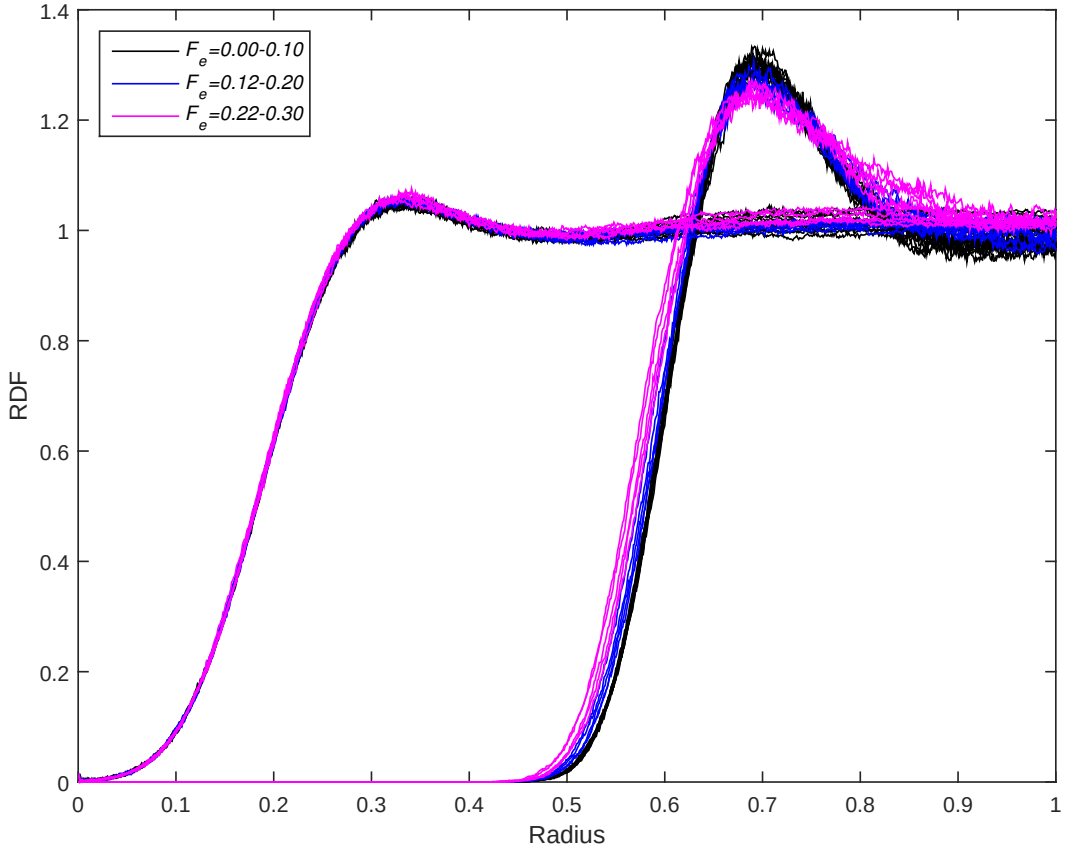

Figure 8: Flows past a periodic array of cylinders, $n = 8$: Fluid-fluid (left) and fluid-cylinder (right) radial distribution functions for different imposed body forces $F_e = (0,\ 0.01,\ 0.02, \cdots,\ 0.10,\ 0.12, \cdots,\ 0.30)$. Their sizes are generally well maintained over the range of the body force applied.

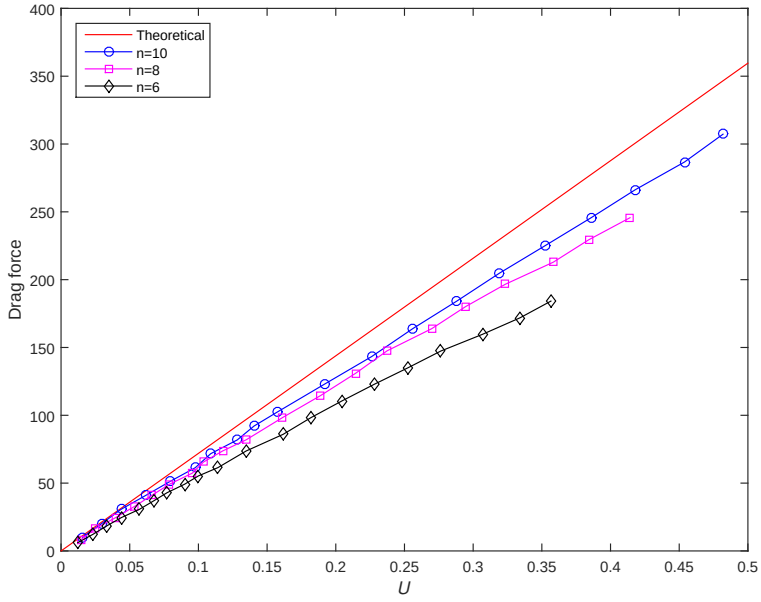

Figure 9: Flows past a periodic array of cylinders: Drag forces against the mean flow velocity U for three coarse-graining levels with the body forces imposed as $F_e = (0.01, 0.02, \cdots, 0.10, 0.12, \cdots, 0.30)$. The three cases have similar behaviours in trend and their values are in better agreement as U is reduced.

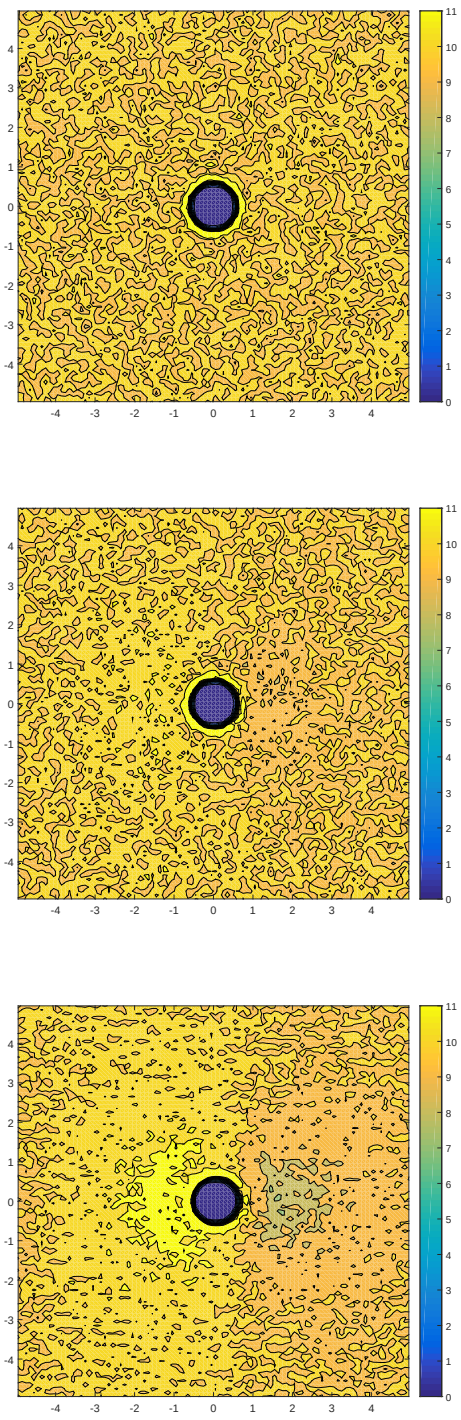

Figure 10: Flows past a periodic array of cylinders, $n = 10$: Distribution of the number density in a cell for 3 typical values of the imposed body force ($F_e = 0$ top; $F_e = 0.1$ middle, and $F_e = 0.3$ bottom). Attention is needed for large F_e values due the effect of compressibility of the model fluid.

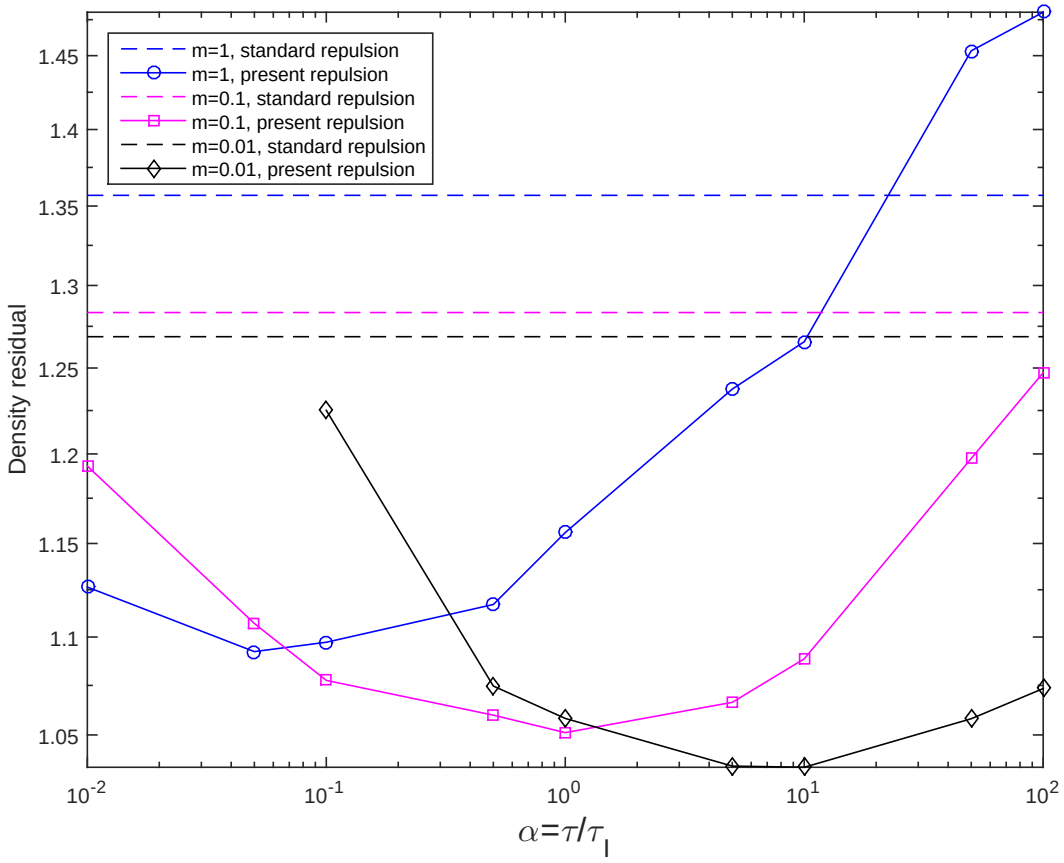

Figure 11: Couette flows, $\eta = 100$, $n = 10$, $\Delta t = 0.0001$, simulation box with dimensions of 10×10, $U = 1$, $r_c = 1.6$, $k_B T = 1$, 100 bins per unit area and 10^6 time steps: Density residual against time-scale ratio for 3 typical values of m. Values of α used are $(10^{-2}, 5 \times 10^{-2}, 10^{-1}, 5 \times 10^{-1}, \cdots, 10^2)$. Results with the standard repulsion are also included. Changing the value of α can lead to a significant improvement in the distribution of number density over the flow domain.

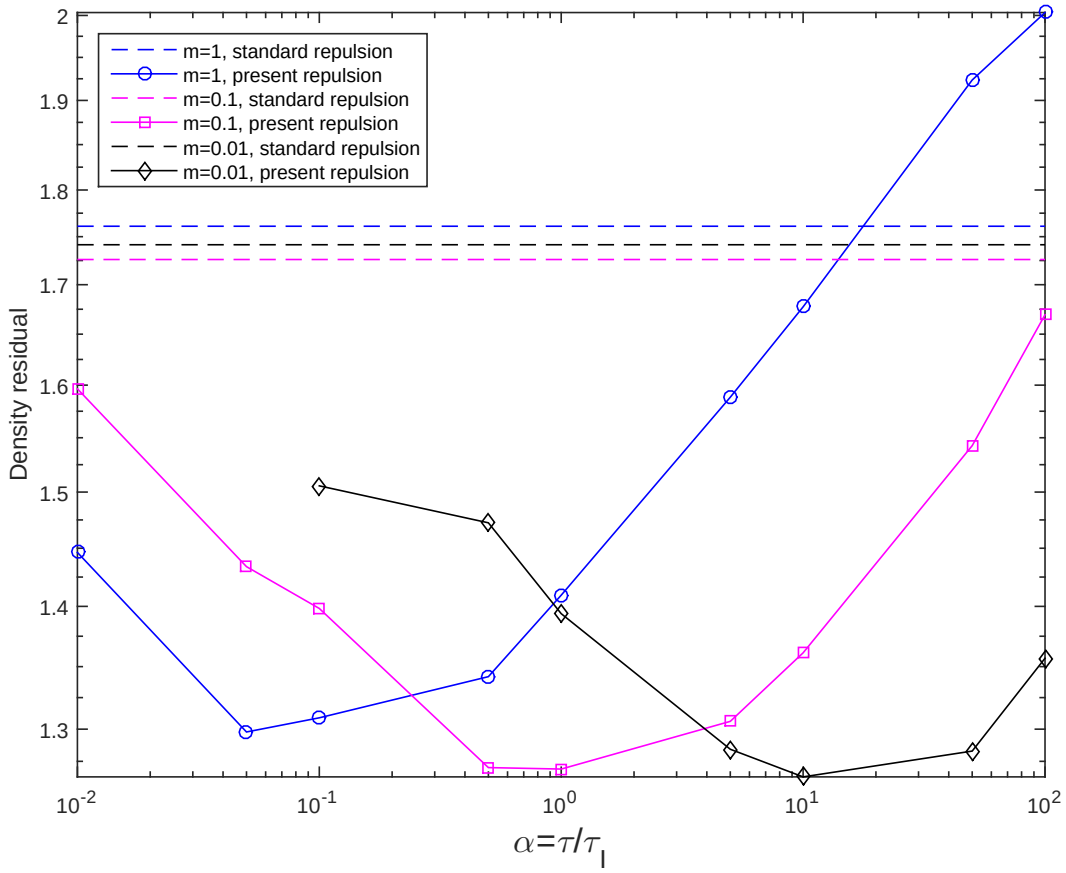

Figure 12: Flows past a periodic square of cylinders, $\eta = 100$, $n = 10$, $\Delta t = 0.0001$, simulation box with dimensions of 10×10, $F_e = 0.3$, $r_c = 1.6$, $k_BT = 1$, 100 bins per unit area and 10^6 time steps: Density residual against time-scale ratio for 3 typical values of m. Values of α used are $(10^{-2}, 5 \times 10^{-2}, 10^{-1}, 5 \times 10^{-1}, \cdots, 10^2)$. Results with the standard repulsion are also included. Changing the value of α can lead to a significant improvement in the distribution of number density over the flow domain.

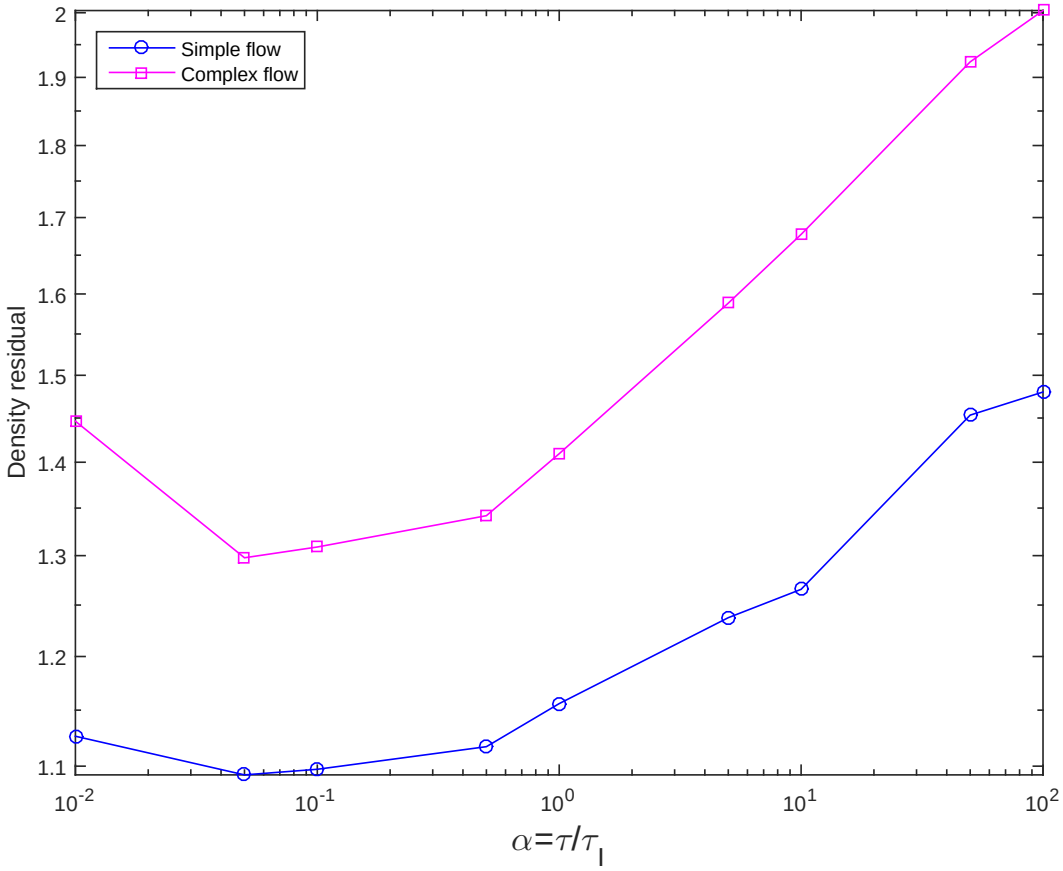

Figure 13: Density residual against time-scale ratio for Couette flows ($U = 1$) and flows past a periodic square array of cylinders ($F_e = 0.3$) with $\eta = 100$, $n = 10$, $\Delta t = 0.0001$, simulation box with dimensions of 10×10, $r_c = 1.6$, $k_BT = 1$, 100 bins per unit area and 10^6 time steps. Values of α used are $(10^{-2}, 5 \times 10^{-2}, 10^{-1}, 5 \times 10^{-1}, \cdots, 10^2)$. The two flows have similar optimal values of α.